This is a repository copy of *3D ultrastructural organisation of calcium release units in the avian sarcoplasmic reticulum*.

White Rose Research Online URL for this paper:
http://eprints.whiterose.ac.uk/143084/

Version: Accepted Version

1   **3D ultrastructural organisation of calcium release units in the avian sarcoplasmic reticulum**

2

3   Thomas M. D. Sheard[1]^, Sanjay R. Kharche[1,2,3], Christian Pinali[1] and Holly A. Shiels[1]*

4

5   [1]University of Manchester, Faculty of Biology, Medicine and Health, Oxford Road, Manchester, M13

6   9PL, United Kingdom

7   [2]Department of Medical Biophysics, University of Western Ontario, London, N6A 3K7, Canada

8   [3] Lawson Health Research Institute, 800 Commissioners Road East, London, Ontario, N6C 2R5,

9   Canada

10

11   **Corresponding authors:**

12   *Holly Shiels, CTF Building, Grafton Street, Manchester M13 9PL, UK.

13   holly.shiels@manchester.ac.uk (Holly A. Shiels);

14   ^Thomas Sheard, present address: University of Leeds, Garstang Building, Woodhouse Lane, Leeds,

15   LS2 9JT, UK. tommichaelsheard@gmail.com (Thomas M. D. Sheard)

16

17

18

19   **Running title:** Calcium release units in avian cardiomyocytes

20

21   **Keywords:** bird, chicken, computational model, calcium diffusion, electron tomography, peripheral

22   coupling

23

24   **Summary statement:** We used electron tomography to create 3D reconstructions of calcium release

25   units in the avian heart. We combined measurements with computer modelling to infer structure-

26   function relationship pertinent to excitation-contraction coupling.

27

28

29   **Abbreviations**

30   Ca^{2+} - calcium / CRU - calcium release unit / SR - sarcoplasmic reticulum / PC - peripheral coupling / cSR - corbular SR / LTCC

31   - L-type calcium channel / RyR - ryanodine receptor / jSR - junctional SR / CICR - calcium-induced calcium release / EjSR -

32   extended junctional SR / ET - electron tomography / TEM - transmission electron microscopy / fSR - free SR / LA - left

33   atrium / RA - right atrium / LV - left ventricle / RV - right ventricle

Abstract

Excitation-contraction coupling in vertebrate hearts is underpinned by calcium (Ca^{2+}) release from Ca^{2+} release units (CRUs). CRUs are formed by clusters of channels called ryanodine receptors on the sarcoplasmic reticulum (SR) within the cardiomyocyte. Distances between CRUs influence the diffusion of Ca^{2+}, thus influencing the rate and strength of excitation-contraction coupling. Avian myocytes lack T-tubules, thus Ca^{2+} from surface CRUs (peripheral couplings, PCs), must diffuse to internal CRU sites of the corbular SR (cSR) during centripetal propagation. Despite this, avian hearts achieve higher contractile rates and develop greater contractile strength than many mammalian hearts, which have T-tubules to provide simultaneous activation of the Ca^{2+} signal through the myocyte. We used 3D electron tomography to test the hypothesis that the intracellular distribution of CRUs in the avian heart permits faster and stronger contractions despite the absence T-tubules. Nearest edge-edge distances between PCs and cSR, and geometric information including surface area and volumes of individual cSR, were obtained for each cardiac chamber of the White Leghorn chicken. Computational modelling was then used to establish a relationship between CRUs distances and cell activation time in the avian heart. Our data suggest that cSR clustered close together along the Z-line is vital for rapid propagation of the Ca^{2+} signal from the cell periphery to the cell centre which would aid in the strong and fast contractions of the avian heart.

1. Introduction

The four-chambered avian heart possesses many similarities to its mammalian counterpart. Both groups independently evolved a fully divided ventricle, capable of producing fast contractile rates with robust pressure development. However, despite similarities in cardiac performance and gross organ morphology, there are substantial differences on a cellular and subcellular level within the cardiomyocytes. Avian atrial and ventricular myocytes are long (>100 μm) and thin (3-9 μm), with a small cross-sectional area (~56 μm^2) and cell volume (~10 pL); these features provide a large surface area to volume ratio (Akester, 1981; Bogdanov *et al.*, 1995; Dzialowski and Crossley II, 2015). It is likely that these morphological features allow excitation-contraction coupling to work within the necessary timescale without sarcolemmal invaginations, known as T-tubules (Sommer and Johnson, 1969). T-tubules are found in all mammalian ventricular myocytes and in atrial myocytes of large mammals, and are important for synchronised depolarisation in these larger cells (Dibb *et al.*, 2009). The lack of T-tubules, characteristic of ectothermic vertebrates (fish, amphibians and non-avian reptiles), has been associated with slower heart rates and less robust contractile function (Shiels and

67   Galli, 2014). We hypothesise that the subcellular organization of calcium (Ca^{2+}) release units (CRUs)

68   within the avian myocyte may reconcile this apparent enigma.

69   Contraction and relaxation of the heart is underpinned by Ca^{2+} cycling in the cardiomyocytes.

70   Following membrane depolarisation, Ca^{2+} enters the cell via voltage-gated L-type Ca^{2+} channels

71   (LTCC). The initial Ca^{2+} that enters via LTCCs induces further Ca^{2+} release from the intracellular stores

72   of the sarcoplasmic reticulum (SR), in a process called Ca^{2+}-induced Ca^{2+} release (CICR). SR Ca^{2+} is

73   released by the ryanodine receptor (RyR) channels, which cluster in structures defined as CRUs. In

74   birds, there are 2 types of CRUs. The first are peripheral couplings (PCs), which are clusters of RyRs

75   on the surface of junctional SR (jSR), directly adjacent to sarcolemmal LTCCs. The second type of CRU

76   is formed by RyR clusters which are not associated with the surface sarcolemma, known as corbular

77   SR (cSR) (also referred to as extended jSR, EjSR). cSR are shorter, rounder segments of SR than those

78   found at the PCs. Despite being positioned micrometres from the sarcolemma (Sommer, 1995),

79   these internal CRUs contribute to global Ca^{2+} release and are necessary for robust excitation-

80   contraction coupling (Franzini-Armstrong *et al.*, 2005). Ca^{2+} released at PCs must diffuse centripetally

81   to the cSR/EjSR. Ca^{2+} is taken up by contracting myofilaments and adjacent mitochondria, or can be

82   buffered in the cytosol, and thus [Ca^{2+}] falls rapidly the further it travels from a CRU (Sobie *et al.*,

83   2006). The distribution of CRUs, as well as the depletion of SR Ca^{2+} stores, ensures that excitation-

84   contraction coupling is not endlessly regenerative and unstable, a situation that would be pro-

85   arrhythmic and deleterious to the myocyte (Cannell *et al.*, 1995).

86   There is a limited amount of functional data on Ca^{2+} flux pathways in avian cardiomyocytes. [^{3}H]

87   ryanodine binding studies in pigeon and finch left ventricle (LV) indicate the density of RyRs and the

88   Ca^{2+} sensitivity of RyRs are similar to mammals (Junker *et al.*, 1994). An early study showed a high

89   density of LTCC current and a prominent T-type Ca^{2+} channel current in whole-cell voltage clamped

90   finch ventricular myocytes (Bogdanov *et al.*, 1995), which the authors suggested could aid in CICR in

91   the absence of T-Tubules. This same study reported faster inactivation kinetics of I_{Ca} in finch

92   compared with rat myocytes and suggested that this may facilitate fast heart rates.

93   We are unaware of studies that quantify the dynamics of avian intracellular Ca^{2+} movement directly

94   (Kim *et al.*, 2000), but it is possible to speculate on this by examining Ca^{2+} cycling in other cells that

95   are similar in structure. Ectotherms, mammalian neonatal cardiomyocytes, and mammalian nodal

96   and Purkinje cells also lack T-tubules and tend to be thinner in diameter than mammalian ventricular

97   cardiomyocytes. Studies from these cell types show that Ca^{2+} levels rise rapidly at the periphery,

98   followed by a time-dependent rise in the cell centre (Boyden *et al.*, 2000; Woo *et al.*, 2003; Shiels

99   and White, 2005; Stuyvers *et al.*, 2005; Louch *et al.*, 2015).

Our current understanding of structural organization of the Ca^{2+} release system in birds discussed above has been characterised using 2D transmission electron microscopy (TEM) (Franzini-Armstrong *et al.*, 1999; Perni *et al.*, 2012). However, a more realistic representation of the CRU distribution in space can be achieved with 3D electron microscopy. In this study we characterise the distribution of CRUs in myocytes from each of the four chambers of the heart of the White Leghorn chicken (*Gallus gallus domesticus*) using electron tomography (ET). This technique enables the reconstruction and visualisation of subcellular organisation of the SR network in a detailed 3D structure. Tomograms from both atria and both ventricles were reconstructed, and the structures of interest were segmented to 1) study the nearest edge-edge distances between PCs and between cSR; and 2) to obtain cSR volumes and surface areas to determine Ca^{2+} capacity and RyR cluster size. These inter-CRU distances were used in to inform a computer model of Ca^{2+} wave dynamics which tested the effect of inter-CRU distances on whole cell Ca^{2+} activation.

2. Methods

2.1 Tissue samples and specimen preparation

Three adult chickens (White Leghorn variety, *Gallus gallus domesticus*; 1.5-2 kg in body mass) were acquired from Hinchliffe's Farm, Huddersfield, UK. White Leghorns are a slow-growing bird, bred for egg production with no pre-disposition to cardiac dysfunction (Mirsalimi *et al.*, 1993). Chickens were transported to the University of Manchester Biological Services Facility where they were humanely euthanised with pentobarbital, followed by dislocation of the neck in accordance with Scientific Procedures Act 1986. Hearts were excised, and tissue from each of the four chambers (left atria, LA; right atria, RA; left ventricle, LV; right ventricle, RV) was cut into 1 mm^3 samples and placed into Karnovsky fixative with $CaCl_2$ (2% formaldehyde, 2.5% glutaraldehyde, 50mM $CaCl_2$, 0.1M HEPES). Tissue preparation was according to the Ellisman protocol (Deerinck *et al.*, 2010). All reagents were obtained from Sigma.

Sectioning was carried out on a Reichert-Jung UltraCut E ultramicrotome using a glass knife. Sections of ~100 nm thickness (gold coloured ribbons) were produced for observation using a FEI Tecnai 12 Bio Twin transmission electron microscope operated at 100 kV to assess tissue preparation prior to electron tomography (ET).

2.2 Electron tomography

Electron tomography (ET) was performed using an FEI Tecnai G2 Polara transmission electron microscope at the University of Manchester Electron Microscopy Facility, operated at 300 kV using

132   magnifications of approximately x10,000, x12,000, and x15,500. For ET, sections of ~400 nm
133   thickness (green/purple coloured ribbons) were collected on 200 mesh grids. 10 nm gold fiducial
134   markers were added to the sections to aid tilt series collection, alignment and data set
135   reconstruction. Tilt series were taken at areas where the myofibrils were longitudinal, as this aids
136   the identification of the cSR. Single-axis tilt series were acquired at 1° intervals from -60° to +60°, or
137   as close to this maximal angle range as possible. Tilt series were obtained from multiple cells within
138   each of the atria and ventricles for all individuals. Alignment, reconstruction and segmentation were
139   performed in the open-source software package *IMOD* (Kremer *et al.*, 1996). *eTomo* was used for
140   alignment and reconstruction, and *3dmod* was used to view the tomograms, segment the structures
141   of interest and to obtain the distances, volumes, and surface area measurements from the 3D
142   reconstructions.

143   Following manual segmentation, the edge-edge distances between the CRUs were measured. PCs
144   were identified as specialised regions of SR in close apposition (10-15 nm) to the sarcolemma (Junker
145   *et al.*, 1994), while cSR were identified as spherical structures (~100 nm in diameter) attached to the
146   SR network, predominantly found along Z-lines (Asghari *et al.*, 2009). Nearest edge-edge distances
147   between PCs and between cSR were obtained from *IMOD* by drawing a line in the tomogram volume
148   between the segmented CRUs. Nearest edge-to-edge distances are important for understanding
149   cellular Ca^{2+} dynamics as they indicate the minimum distance that must be crossed by Ca^{2+} released
150   at one site in order to act on an adjacent site (Perni *et al.*, 2012). Since cSR are distributed around
151   the Z-lines, we measured distances between cSR distributed around the same Z-line. Geometric data
152   regarding individual cSR were obtained by fully segmenting each cSR in every slice of each
153   tomogram.

154

155   **2.3 Computational methods**

156   *2.3.1. Model geometry*

157   A 2D Ca^{2+} wave model representing an avian cardiomyocyte was constructed to assess the
158   relationship between inter-CRU distances and whole cell Ca^{2+} activation times. The myocyte was
159   constructed as 8 μm wide (Y axis) and 136 μm long (X axis) (Kim *et al.*, 2000). PCs were placed at
160   regular intervals along the cell membrane in the X direction; Z-lines were placed at regular intervals
161   along the X axis and extended across the Y axis, and cSR were placed at regular intervals on the Z-
162   lines (see Fig. 5A). The model geometry was discretised at a space step of 0.05 μm and thus PCs were
163   placed at a depth from the cell membrane of 50 nm. This is greater than the biological distance (~
164   10-15 nm) but we were required to accept this limitation due to the computational power required

165 to provide finer discretisation. CRUs were separated by distances d1 (distance between PCs), d2

166 (distance between Z-lines), d3 (distance between cSR along a Z-line). These distances were varied in

167 a systematic way to encompass the range of values measured in the tomogram datasets. Distance

168 d1 was tested at 0.25, 0.5 and 0.75 µm, d3 at 0.1, 0.2, 0.4, 0.6 µm, and d2 was varied to represent Z-

169 line spacing indicative of a myocyte at rest (1.7-1.9 µm), as well as encompassing values that could

170 be achieved during myocardial stretch (2.1 µm) and myocardial contraction (1.5 µm). The ranges of

171 distances are tabulated in the Table S1.

172

173 *2.3.2. Ca^{2+} dynamics model*

174 The Ca^{2+} dynamics model was adapted from previous models (Cheng *et al.*, 1993; Smith *et al.*, 1998;

175 Izu *et al.*, 2001). CRU activation began at the surface sarcolemma and moved towards the centre of

176 the cell. Cell membrane activation initiated propagation of the Ca^{2+} wave in the Y direction. At t = 0,

177 [Ca^{2+}] was raised to 100 µM at Y = 0 µm and Y = 8 µm for 1 ms. Ca^{2+} dynamics were then permitted

178 to evolve for the duration of 1 heartbeat (225 ms), according to the equations given in *2.3.3*. Whole

179 cell activation was achieved when all grid locations reached a [Ca^{2+}] value of 100 µM or more at least

180 once (as per Smith *et al.*, 1998; Izu *et al.*, 2001). Ca^{2+} release was simulated as a stochastic process,

181 release at a CRU occurred when local [Ca^{2+}] exceeded 0.1 µM as described previously (Smith *et al.*,

182 1998). The probability of a given CRU being open was assumed to be proportional to *Jpump* (see

183 below). Once a CRU was open, it was permitted to release Ca^{2+} for 10 ms (Smith *et al.*, 1998). The

184 spatial network of CRUs were diffusively coupled to permit simulation of Ca^{2+} waves (Izu *et al.*,

185 2001).

186

187 The effect of mobile buffers was omitted. This may affect the absolute slope of the relationship

188 between Ca^{2+} activation time and the distances between CRUs, but is not expected to impact the

189 relative effect of changing distance (d1, d2 and d3) on activation time.

190

191 Robust implicit finite difference solvers developed previously (Kharche *et al.*, 2017) were used to

192 solve the reaction-diffusion equations using a maximum temporal step of 0.02 ms (Table S1). Ten

193 simulations were performed for each combination of distances (d1, d2, d3), and an average

194 activation time from the 10 simulations was taken to form each data point. Parallelisation was

195 implemented using message passing interface (MPI). Each simulation required 24 processors 4 hours

196 to complete.

197

198 *2.3.3. Model equations for Ca^{2+} wave propagation simulations.*

199 <mark>Model equations were derived from those found in equation 2 of Izu et al (Smith *et al.*, 1998; Izu *et*</mark>

200 <mark>*al.*, 2001).</mark>

201

$$\frac{\partial [Ca^{2+}]_i}{\partial t} = D_c \nabla^2 [Ca^{2+}]_i + J_{buffers} + J_{pump} + J_{leak} + J_{ryr} \quad \text{Eq. 1}$$

$$\frac{\partial [CaB_n]}{\partial t} = -J_n \qquad \qquad \text{(immobile buffers)} \qquad \text{Eq. 2}$$

$$J_n = -k_n^+ [Ca^{2+}]_i ([B_n]_{total} - [CaB_n]) + k_n^- [CaB_n] \quad \text{Eq. 3}$$

$$J_{pump} = \frac{v^{max}_{pump} [Ca^{2+}]_i^m}{K^m_{pump} + [Ca^{2+}]_i^m}, \quad m = 3.98 \qquad \qquad \text{Eq. 4}$$

$$J_{leak} = -J_{pump}(c_\infty) = -\frac{v^{max}_{pump} c_\infty^m}{K^m_{pump} + c_\infty^m}, \quad c_\infty = 0.1\ \mu M \quad \text{Eq. 5}$$

$$J_{ryr} = O \times \sigma_{ryr} \qquad \text{at CRU locations.} \qquad \qquad \text{Eq. 6}$$

203

204 J_{ryr} is the Ca^{2+} released by the CRU, σ_{ryr} is a 10 ms pulse of 2 pA amplitude injected into the medium

205 by the RyR at CRU location. The variable O took values of 1 or 0 depending on whether the CRU was

206 open or not respectively, and was determined stochastically. The probability of O being open was

207 assumed to be proportional to *Jpump*. Once assigned a value of 1, O retained the value for 10 ms,

208 the open time for the CRU (Smith *et al.*, 1998).

209

210 **2.4 Statistics**

211 Statistics were performed using *GraphPad Prism* with unpaired t-tests and one-way ANOVAs, with

212 Tukey post hoc analysis as specified in the figure legends. The threshold for statistical significance

213 was $P < 0.05$. The results are expressed as mean ± s.e.m., with the number of measurements, from

214 the number of tissues sections and the number of animals, provided in each legend. The spread of

215 data is shown using scatter plots of individual data points with mean values overlaid.

216

217 **3. Results**

218 **3.1 Segmented model for calculating distances**

219 Each tomogram is a reconstruction of an approximately 400 nm thick section of avian cardiac tissue

220 (Fig. 1; Movie S1). When the tissue <mark>is sectioned</mark> longitudinally with respect to the axis of the cells, it

221 is apparent that cSR <mark>(yellow)</mark> are localised at the Z-lines and thus are separated at roughly the length

222   of the sarcomere (Fig. 1A,B). The 3D structural model (Fig. 1C; Movie S2) gives a representative

223   display of cSR spread along Z-lines, as well as the entire SR network adjacent to the sarcolemma.

224   *3.1.1 Peripheral couplings*

225   PCs are defined as clusters of RyRs on the surface of the jSR which are directly adjacent (10-15 nm)

226   to LTCCs on the sarcolemma (Fig. 2A,B). The mean (± s.e.m.) nearest edge-edge distances between

227   PCs in each of the four chambers of the heart were as follows: LA 377 ± 19 nm (n=380), RA 347 ± 22

228   nm (n=228), LV 334 ± 26 nm (n=193), RV 462 ± 30 nm (n=195)(n= number of individual distances

229   measured; Fig. 2C). Distances between PCs in the RV were significantly greater (one-way ANOVA,

230   P<0.05) than those measured in the other cardiac chambers.

231   *3.1.2 Corbular sarcoplasmic reticulum*

232   The internal CRUs in avian hearts are the cSR, which are spherical structures of approximately 100

233   nm diameter, typically found staggered along the Z-line (Fig. 3A,B; Movie S3). cSR are notably larger

234   in size than the network tubules of free SR (fSR), however they are highly polymorphous in their

235   geometry, varying in shape and size (described below). The mean (± s.e.m.) nearest edge-edge

236   distances between cSR at the same Z-line (Fig. 3C) in each of the four chambers of the heart were as

237   follows: LA 423 ± 16 nm (n=286), RA 501 ± 20 nm (n=189), LV 485 ± 24 nm (n=133), RV 465 ± 23 nm

238   (n=194). Distances measured in LA were significantly shorter than in RA but not different from the

239   two ventricles (one-way ANOVA P<0.05).

240

241   **3.2 Geometric models for individual corbular sarcoplasmic reticulum**

242   ET enables the 3D rendering of structures of interest (Fig. 4A,B). Thus diameter (Fig. 4C), surface area

243   (Fig. 4D) and volume (Fig. 4E) of cSR in each chamber of an individual bird heart was measured to

244   provide insight into their role in Ca^{2+} release (Table S2). The scatterplots (Fig. 4C,D,E) highlight the

245   polymorphic nature of the geometry of bird cSR. The LA cSR were smaller (one-way ANOVA P<0.05)

246   in volume and surface area than the other chambers.

247

248   **3.3 Computational modelling Ca^{2+} dynamics**

249   To understand how inter-CRU distances may impact on Ca^{2+} activation time in an avian myocyte

250   devoid of T-tubules, we constructed a spatially extended 2D Ca^{2+} wave model. In the model, CRUs

251   were placed at locations separated by distances d1 (distance between PCs), d2 (distance between Z-

252   lines), d3 (distance between cSR along a Z-line) (Fig. 5A). Frames from a simulation of Ca^{2+} waves

253 show the mode of diffusion across the cell, $[Ca^{2+}]$ initially increasing at the periphery before diffusion

254 into the interior along the z-lines (Fig. 5B).

255 CRU distances in the model were varied in a systematic way to encompass the range of values

256 measured in the tomograms, in order to deduce the effect on whole cell activation time (Fig. 6). This

257 analysis suggests that distance between PCs (d1) has little effect on whole cell Ca^{2+} activation time

258 (Fig. 6A). In contrast, when the distance between cSR (d3) is increased from 0.1 μm to 0.2 μm,

259 activation time is delayed by approximately 3.5 ms; as d3 is increased to 0.4 μm activation time is

260 more than 10 ms longer than at 0.1 μm (Fig. 6B). At larger d3 distances (beyond those measured

261 between cSR within a Z-line in the current study) activation time is slowed even further. Under these

262 conditions, widely separated PCs (d1) compound the effect and activation time requires

263 approximately 20 ms. In general, activation time is unaffected as distance between Z-lines are varied

264 (d2) in a manner anticipated during sarcomeric stretch and contraction (Fig. 6A,B). Indeed, because

265 the distance d3 was considerably smaller than distance d2, the CRUs along the Z -lines activated

266 prior to Ca^{2+} passively diffusing to neighbouring Z-lines that were not proximal to the PCs.

267

268 **4. Discussion**

269 Aves occupy a unique position in vertebrate evolution. They possess a 4-chambered heart with a

270 fully divided ventricle, which arose independently from that in mammals. However, despite gross

271 structural similarities to mammalian hearts, at a cellular level, the avian cardiomyocyte more closely

272 resembles that of (non-avian) reptiles. This study is the first to use electron tomography to

273 investigate the subcellular distribution of the intracellular Ca^{2+} release machinery in the avian heart.

274 We measured distances between PCs and between cSR along a Z-line, and found the PCs to be closer

275 together and the cSR further apart than those reported previously using 2D TEM (Franzini-Armstrong

276 *et al.*, 1999; Perni *et al.*, 2012). Our study has also revealed the diversity of the cSR volumes and

277 varied distribution of these structures in all four cardiac chambers. We then used a computational

278 approach to test how varying distances between these subcellular CRUs affects Ca^{2+} activation time.

279 Our model highlights the importance of distances between cSR along a Z-line (d3). Together, our

280 findings suggest that cSR clustered close together along the Z-line are vital for rapid propagation of

281 the Ca^{2+} signal from the cell periphery to the cell centre, and facilitate strong and fast contractions.

282

283 **4.1 Peripheral couplings distances**

284 CRUs in the form of PCs have been identified in the hearts of all vertebrates studied, except in the

285 frog ventricle, and are most often associated with the Z-lines (Shiels and Galli, 2014). The mean

286 distances between nearest neighbour PCs in the White Leghorn chicken ranged from 334 nm in LV,

287   to 462 nm in RV, which is comparable to previous values measured using 2D TEM in LV (472 nm
288   (Franzini-Armstrong *et al.*, 1999) and 567 nm (Perni *et al.*, 2012)). We found similar distances
289   between PC in the LV, RA and LA but slightly longer distances in the RV. The functional significance of
290   this pattern is unclear. Size and frequency of peripheral CRUs varies between vertebrate species and
291   between cardiac chambers within a species, and in some studies this variability has been related to
292   the efficacy of excitation-contraction coupling (Perni *et al.*, 2012; Shiels and Galli, 2014). Indeed,
293   animals with high heart rates (i.e. finch and rat, resting heart rate ~300-350 bpm) have closer PCs
294   than animals with slower heart rates (Perni *et al.*, 2012) (i.e. chicken, resting heart rate ~200 bpm;
295   lizard and fish, heart rate dependent on temperature but generally below 120 bpm (Farrell, 1991)).
296   The distances measured in our study supports previous work in chicken (Perni *et al.*, 2012), which
297   suggests PCs are activated by adjacent LTCCs in the sarcolemmal membrane directly, with little
298   spread of activating Ca^{2+} longitudinally between PCs. Indeed, our simulations suggest that changing
299   the distance between PCs between 250 nm and 750 nm has little impact on whole cell activation,
300   particularly when the distances between cSR are narrow (Fig. 6). This differs from mammalian atrial
301   myocytes and from birds with faster heart rates and/or contractile force (i.e. finch (Perni *et al.*,
302   2012)) where extensive and propagative CICR between neighbouring CRUs at the cell periphery has
303   been observed (Chen-Izu *et al.*, 2006). In the finch heart, closely packed PCs are further aided by
304   higher density of LTCCs (Bogdanov *et al.*, 1995) to achieve fast heart rates.

305

4.2 Corbular SR distances

307   The CRUs of the avian cSR can be thought of as Ca^{2+} release relay stations, carrying the wave of Ca^{2+}
308   from the myocyte periphery to the cell centre in the absence of T-tubules. We found the average
309   distance between cSR at the same Z-line to range from 422 nm in LA, to 500 nm in RA, which are
310   significantly larger than those reported by Franzini-Armstrong's group for LV (148 nm (Franzini-
311   Armstrong *et al.*, 1999) and 235 nm (Perni *et al.*, 2012)) using 2D TEM images taken in a transverse
312   section. Franzini-Armstrong et al. state that "larger distances were ignored" in their measurements,
313   so although the exact threshold used for excluding large distances is not specified, it may explain the
314   discrepancy between studies. The heterogeneous distribution of organelles (e.g. mitochondria),
315   combined with changes in distances between organelles during the contraction-relaxation cycle are
316   both features which help prevent circular, endless propagation of a Ca^{2+} wave. Indeed, our
317   computational model indicates that the distance between cSR has a dramatic effect on the
318   activation time. As cSR distances are varied from those measured previously (~150-235 nm) to those
319   measured in our study (~400-500 nm), activation time more than doubles (Fig. 6). Thus, chains of

320 closely distributed cSR at a Z-line increase the probability that Ca^{2+} will be able to diffuse and
321 activate neighbouring units.

322

323 **4.3 Corbular SR Geometry**

324 We provide the first 3D geometrical description of cSR in chicken hearts. A similar diverse and
325 polymorphic description has been detailed for the jSR and the T-tubule lattice in mouse
326 cardiomyocytes (Hayashi *et al.*, 2009). Average diameters for cSR from each of the four chambers
327 ranged from 120-130 nm, a parameter that aided cSR identification. The average volume of a cSR in
328 each of the four chambers ranged from 446,000 - 600,000 nm^3, but the largest and smallest ranged
329 from 120,000 nm^3 to 1,410,000 nm^3. The average surface area from each of the four chambers
330 ranged from 22,000 to 28,000 nm^2 but the extremes were 9,000 nm^2 and 60,000 nm^2. Thus, there is
331 extreme heterogeneity in the avian cardiomyocyte's Ca^{2+} release structures.

332 We were unable to resolve individual RyR positions on the cSR in this study. However, given the
333 average surface area of cSR was between 22,000 to 28,000 nm^2, and knowing that a single RyR is 29
334 x 29 nm^2, or 841 nm^2 (Chen-Izu *et al.*, 2006; Baddeley *et al.*, 2009), we calculate that the average
335 chicken cSR could support between 26-33 RyR molecules. RyRs probably do not occupy the entire
336 cSR surface, for instance the dyad is only partially filled, and RyR clusters often present a
337 checkerboard appearance (Baddeley *et al.*, 2009; Asghari *et al.*, 2014). We therefore estimate the
338 average cSR possesses approximately 13-16 RyRs.

339 Calculations concerning jSR Ca^{2+} capacity (whereby jSR of volume $7x10^{-4}$ μm^3 contains 21,000 Ca^{2+}
340 ions (Sobie *et al.*, 2002)), lead us to suggest the average avian cSR would contain between 13,380
341 and 18,000 Ca^{2+} ions. The minimum and maximum volumes of cSR found here, would thus contain
342 3,600 and 42,300 Ca^{2+} ions respectively. A 1pA current releases around 3,000 ions per millisecond
343 (Sobie *et al.*, 2002), and thus the total capacity of the cSR analysed in this study permits Ca^{2+} release
344 for ~5 ms in total before the SR is depleted of Ca^{2+}. SR Ca^{2+} available for release at these CRUs is
345 replenished by SERCA Ca^{2+} uptake along the fSR network, which diffuses back towards the junctional
346 area containing the RyRs. Thus the total capacity of the cSR does not finitely dictate the duration of
347 Ca^{2+} release. It is likely that the total capacity can be released in the order of tens of milliseconds,
348 correlating with previous measurements for known spark durations (Sobie *et al.*, 2002; Stern *et al.*,
349 2013) although the actual spark duration in avian cardiomyocytes is not known. These estimates
350 correlate with the Ca^{2+} activation time of our model which ranges between 5 and 25 ms, with mean
351 ~15 ms, for the whole cell to be activated, depending on CRU spacing.

352

4.4 Ca^{2+} dynamics model

We used a spatially extended 2D cell model to improve the interpretation of our experimental data. The model showed that the variation of distances between cSR within a Z-line supersedes that of distances between PCs at the cell membrane for setting Ca^{2+} activation time of the cell. Our model has limitations that need to be considered when interpreting our results. First, stimulation was assumed to be generated by a rapidly propagating electrical pulse along the length of the cardiomyocyte membrane. Therefore, the initiated Ca^{2+} wave had an inward propagation. Thus, barring any numerical and boundary condition effects, it may be expected that PCs played a limited role in the output of whole cell Ca^{2+} activation. Our model also incorporated local stochastic Ca^{2+} release, or sparks. The Ca^{2+} released by the sparks diffused in the cytoplasm uniformly in all directions; thus the Ca^{2+} diffusing from a cSR would stimulate release from the directly adjacent CRU along the same Z-line prior to stimulating other CRUs. In previous studies, inter-CRU distances were assumed to be uniform in both X and Y direction, thus the work here extends these earlier models (Izu *et al.*, 2001; Izu *et al.*, 2013). However, in our model the locations of the CRUs were assumed to be symmetric, which aligns with the positioning along the Z-lines that we observed experimentally in the bird heart. However, stochasticity in the spatial distribution of CRUs has been observed (Qu *et al.*, 2014), and will be included in future studies. Lastly, due to the limited functional studies of Ca^{2+} dynamics in avian myocytes (Kim *et al.*, 2000), the model was parameterised based on mammalian data. Further functional studies are need to accurately measure Ca^{2+} flux in avian cardiomyocytes. Improved numerical schemes and solvers are also required to permit exploration of the experimental data in more depth. However, peak systolic Ca^{2+} is reached in a similar time frame and at a similar level in our model and that in mammals (Bers, 2002), despite the difference in cell structure between species.

4.5 Perspectives for avian cardiac performance

Domestic chickens have an average heartbeat of 218 beats min^{-1} (Prosheva *et al.*, 2015). A single cardiac cycle is ~0.275 s comprised of the following electrocardiogram components: P wave (atrial depolarisation) ~30 ms, PQ interval ~60 ms (AV-conduction), QRS (ventricular depolarisation) ~30 ms, and QT interval (duration ventricular action potential) ~140 ms (Prosheva *et al.*, 2015). Ca^{2+} release follows the depolarising wave and thus our mean Ca^{2+} activation time of 12-20 ms is within a reasonable range. In the scenario where cSR distances are at or beyond the level we observed in our tomographic data, activation time would be closer to 25-30 ms. However, in vivo the rate of Ca^{2+} removal and SR replenishment will also influence the speed of the calcium cycle, as

386 increase/decrease in heart rate is predominantly dictated by the duration of the interval between T
387 and P waves (Dzialowski and Crossley II, 2015). Functional studies are required in avian myocytes to
388 reveal the complexities of Ca^{2+} signalling in this cell type, for instance the speed of Ca^{2+} extrusion,
389 and specific channel currents.

390

391 In birds with faster heart rates, such as the finch or hummingbird, rapid cardiac contraction relies on
392 even faster relaying of the Ca^{2+} signal. This is brought about by closer spacing of CRUs, and in the
393 case of the finch heart, existence of EjSR in place of cSR (Perni et al., 2012). EjSR are more elongated
394 CRUs, which might offer a greater capacity for Ca^{2+} storage, increased numbers of RyRs per cluster
395 for Ca^{2+} release, or a better geometry for the spread of signal to neighbouring sites.

396

397 **5. Summary**
398 Our measurements of distances between PCs and cSR, coupled with computational simulations,
399 suggest that in chicken cardiomyocytes the Ca^{2+} transient would be initiated at the periphery, be
400 large in concentration around this sub-sarcolemmal space, and diffuse toward the interior along
401 chains of cSR. The resulting effect would be spatial inhomogeneity and nonsynchronous spread of
402 Ca^{2+} across the whole myocyte. However, upon activation of many CRUs, given that Ca^{2+} is of large
403 enough magnitude, diffusion between cSR positioned at adjacent Z-lines is possible, becoming more
404 probable the closer they are to one another. This pattern is similar to that found in neonatal
405 mammalian myocytes (Louch et al., 2015). As noted by others previously (Perni et al., 2012), the
406 extensive and almost exclusive location of cSR along the Z-lines in bird myocytes induces a high
407 degree of refractoriness to longitudinal Ca^{2+} wave propagation, with activation initiated
408 independently at PCs cascading through the cSR. Thus, the organization of CRUs and the short
409 diffusional distance for Ca^{2+} transport in narrow cells allows for strong and fast contractions in avian
410 myocytes and reinforces the connection between structural organization of the myocyte, the CRUs,
411 and the strength and rate of cardiac contraction across vertebrate classes.

412

413 **Competing interests**
414 We have no competing interests.

415

416 **Author Contributions**

417 TS, CP, and HS designed the experimental study. TS carried out the experiments, imaging, and
418 analysed data. CP assisted in data analysis. SRK constructed the model, incorporated the

419 experimental data, designed, and performed the simulations. All authors contributed to
420 interpretation of the simulation results, writing the manuscript and approved the final version.

421

431
432
433 **References**

434
435 AKESTER, A. R. 1981. Intercalated discs, nexuses, sarcoplasmic reticulum and transitional cells in the
436   heart of the adult domestic fowl (Gallus gallus domesticus). *J Anat,* 133, **,** 161-79.
437 ASGHARI, P., SCHULSON, M., SCRIVEN, D. R. L., MARTENS, G. & MOORE, E. D. W. 2009. Axial
438   Tubules of Rat Ventricular Myocytes Form Multiple Junctions with the Sarcoplasmic
439   Reticulum. *Biophysical Journal,* 96, **,** 4651-4660.
440 ASGHARI, P., SCRIVEN, D. R. L., SANATANI, S., GANDHI, S. K., CAMPBELL, A. I. M. & MOORE, E. D.
441   W. 2014. Nonuniform and Variable Arrangements of Ryanodine Receptors Within
442   Mammalian Ventricular Couplons. *Circulation Research,* 115, **,** 252-262.
443 BADDELEY, D., JAYASINGHE, I. D., LAM, L., ROSSBERGER, S., CANNELL, M. B. & SOELLER, C. 2009.
444   Optical single-channel resolution imaging of the ryanodine receptor distribution in rat
445   cardiac myocytes. *Proceedings of the National Academy of Sciences,* 106, **,** 22275-22280.
446 BERS, D. M. 2002. Cardiac excitation-contraction coupling. *Nature,* 415, 198-205.
447 BOGDANOV, K. Y., ZIMAN, B. D., SPURGEON, H. A. & LAKATTA, E. G. 1995. L- and T-type calcium
448   currents differ in finch and rat ventricular cardiomyocytes. *J Mol Cell Cardiol,* 27, **,** 2581-93.
449 BOYDEN, P. A., PU, J., PINTO, J. & TER KEURS, H. E. D. J. 2000. Ca(2+) Transients and Ca(2+) Waves
450   in Purkinje Cells Role in Action Potential Initiation. *Circulation research,* 86, **,** 448-455.
451 CANNELL, M. B., CHENG, H. & LEDERER, W. J. 1995. The control of calcium release in heart muscle.
452   *Science,* 268, **,** 1045-9.
453 CHEN-IZU, Y., MCCULLE, S. L., WARD, C. W., SOELLER, C., ALLEN, B. M., RABANG, C., CANNELL, M.
454   B., BALKE, C. W. & IZU, L. T. 2006. Three-dimensional distribution of ryanodine receptor
455   clusters in cardiac myocytes. *Biophys J,* 91, **,** 1-13.
456 CHENG, H., LEDERER, W. J. & CANNELL, M. B. 1993. Calcium sparks: elementary events underlying
457   excitation-contraction coupling in heart muscle. *Science,* 262, **,** 740-4.

458 **DEERINCK, T. J., BUSHONG, E., THOR, A. & ELLISMAN, M. H.** 2010. NCMIR methods for 3D EM: a
459   new protocol for preparation of biological specimens for serial block face scanning electron
460   microscopy.
461 **DIBB, K. M., CLARKE, J. D., HORN, M. A., RICHARDS, M. A., GRAHAM, H. K., EISNER, D. A. &**
462   **TRAFFORD, A. W.** 2009. Characterization of an extensive transverse tubular network in
463   sheep atrial myocytes and its depletion in heart failure. *Circ Heart Fail,* 2**,** 482-9.
464 **DZIALOWSKI, E. M. & CROSSLEY II, D. A.** 2015. Chapter 11 - The Cardiovascular System. *In:* SCANES,
465   C. G. (ed.) *Sturkie's Avian Physiology (Sixth Edition).* San Diego: Academic Press.
466 **FARRELL, A. P.** 1991. From Hagfish to Tuna: A Perspective on Cardiac Function in Fish. *Physiological*
467   *Zoology,* 64**,** 1137-1164.
468 **FRANZINI-ARMSTRONG, C., PROTASI, F. & RAMESH, V.** 1999. Shape, size, and distribution of Ca(2+)
469   release units and couplons in skeletal and cardiac muscles. *Biophysical Journal,* 77**,** 1528-
470   1539.
471 **FRANZINI-ARMSTRONG, C., PROTASI, F. & TIJSKENS, P.** 2005. The assembly of calcium release units
472   in cardiac muscle. *Ann N Y Acad Sci,* 1047**,** 76-85.
473 **HAYASHI, T., MARTONE, M. E., YU, Z., THOR, A., DOI, M., HOLST, M. J., ELLISMAN, M. H. &**
474   **HOSHIJIMA, M.** 2009. Three-dimensional electron microscopy reveals new details of
475   membrane systems for Ca2+ signaling in the heart. *J Cell Sci,* 122**,** 1005-13.
476 **IZU, L. T., WIER, W. G. & BALKE, C. W.** 2001. Evolution of cardiac calcium waves from stochastic
477   calcium sparks. *Biophys J,* 80**,** 103-20.
478 **IZU, L. T., XIE, Y., SATO, D., BÁNYÁSZ, T. & CHEN-IZU, Y.** 2013. Ca(2+) waves in the heart. *Journal of*
479   *molecular and cellular cardiology,* 58**,** 118-124.
480 **JUNKER, J., SOMMER, J. R., SAR, M. & MEISSNER, G.** 1994. Extended junctional sarcoplasmic
481   reticulum of avian cardiac muscle contains functional ryanodine receptors. *J Biol Chem,* 269**,**
482   1627-34.
483 **KHARCHE, S. R., VIGMOND, E., EFIMOV, I. R. & DOBRZYNSKI, H.** 2017. Computational assessment of
484   the functional role of sinoatrial node exit pathways in the human heart. *PLoS One,* 12**,**
485   e0183727.
486 **KIM, C. S., DOYE, A. A., GWATHMEY, J. K., DAVIDOFF, A. J. & MAKI, T. M.** 2000. Intracellular calcium
487   and the relationship to contractility in an avian model of heart failure. *Journal of*
488   *comparative physiology. B, Biochemical, systemic, and environmental physiology,* 170**,** 295-
489   306.
490 **KREMER, J. R., MASTRONARDE, D. N. & MCINTOSH, J. R.** 1996. Computer visualization of three-
491   dimensional image data using IMOD. *J Struct Biol,* 116**,** 71-6.
492 **LOUCH, W. E., KOIVUMAKI, J. T. & TAVI, P.** 2015. Calcium signalling in developing cardiomyocytes:
493   implications for model systems and disease. *J Physiol,* 593**,** 1047-63.
494 **MIRSALIMI, S. M., O'BRIEN, P. J. & JULIAN, R. J.** 1993. Blood volume increase in salt-induced
495   pulmonary hypertension, heart failure and ascites in broiler and White Leghorn chickens.
496   *Canadian Journal of Veterinary Research,* 57**,** 110-113.
497 **PERNI, S., IYER, V. R. & FRANZINI-ARMSTRONG, C.** 2012. Ultrastructure of cardiac muscle in reptiles
498   and birds: optimizing and/or reducing the probability of transmission between calcium
499   release units. *J Muscle Res Cell Motil,* 33**,** 145-52.
500 **PROSHEVA, V., DERNOVOJ, B., KHARIN, S., KASEVA, N., SHKLYAR, T. & BLYAKHMAN, F.** 2015. Does
501   the right muscular atrioventricular valve in the avian heart perform two functions?
502   *Comparative Biochemistry and Physiology Part A: Molecular & Integrative Physiology,* 184**,**
503   41-45.
504 **QU, Z., HU, G., GARFINKEL, A. & WEISS, J. N.** 2014. Nonlinear and Stochastic Dynamics in the Heart.
505   *Phys Rep,* 543**,** 61-162.
506 **SHIELS, H. A. & GALLI, G. L.** 2014. The sarcoplasmic reticulum and the evolution of the vertebrate
507   heart. *Physiology (Bethesda),* 29**,** 456-69.

508   **SHIELS, H. A. & WHITE, E.** 2005. Temporal and spatial properties of cellular Ca2+ flux in trout
509   ventricular myocytes. *Am J Physiol Regul Integr Comp Physiol,* 288**,** R1756-66.
510   **SMITH, G. D., KEIZER, J. E., STERN, M. D., LEDERER, W. J. & CHENG, H.** 1998. A simple numerical
511   model of calcium spark formation and detection in cardiac myocytes. *Biophysical journal,* 75**,**
512   15-32.
513   **SOBIE, E. A., DILLY, K. W., DOS SANTOS CRUZ, J., LEDERER, W. J. & JAFRI, M. S.** 2002. Termination of
514   cardiac Ca(2+) sparks: an investigative mathematical model of calcium-induced calcium
515   release. *Biophysical Journal,* 83**,** 59-78.
516   **SOBIE, E. A., GUATIMOSIM, S., GÓMEZ-VIQUEZ, L., SONG, L.-S., HARTMANN, H., JAFRI, M. S. &**
517   **LEDERER, W. J.** 2006. The Ca(2+) leak paradox and "rogue ryanodine receptors": SR Ca(2+)
518   efflux theory and practice. *Progress in biophysics and molecular biology,* 90**,** 172-185.
519   **SOMMER, J. & JOHNSON, E.** 1969. Cardiac muscle. *Zeitschrift für Zellforschung und Mikroskopische*
520   *Anatomie,* 98**,** 437-468.
521   **SOMMER, J. R.** 1995. Comparative anatomy: in praise of a powerful approach to elucidate
522   mechanisms translating cardiac excitation into purposeful contraction. *J Mol Cell Cardiol,* 27**,**
523   19-35.
524   **STERN, M. D., RÍOS, E. & MALTSEV, V. A.** 2013. Life and death of a cardiac calcium spark. *The Journal*
525   *of General Physiology,* 142**,** 257-274.
526   **STUYVERS, B. D., DUN, W., MATKOVICH, S., SORRENTINO, V., BOYDEN, P. A. & TER KEURS, H. E. D.**
527   **J.** 2005. Ca2+ Sparks and Waves in Canine Purkinje Cells: A Triple Layered System of Ca2+
528   Activation. *Circulation Research,* 97**,** 35-43.
529   **WOO, S.-H., CLEEMANN, L. & MORAD, M.** 2003. Spatiotemporal Characteristics of Junctional and
530   Nonjunctional Focal Ca2+ Release in Rat Atrial Myocytes. *Circulation Research,* 92**,** e1-e11.

531

532   **Figure legends**

533   **Fig. 1.** Tomograms and segmented structural models used for measuring inter-CRU distances in
534   avian left atrial tissue. **(A)** 2D image from a reconstructed tomogram stack, with a segmented model
535   overlaid. The segmented model shows: peripheral couplings (PCs) (purple) and the nearest edge-
536   edge distances between PCs (blue lines); corbular sarcoplasmic reticulum (cSR) (yellow) and the
537   nearest edge-edge distances between these CRUs along a Z-line (red lines). Also segmented are the
538   mitochondria (cyan) and the sarcolemma (green lines). Scale bar = 500 nm. Note that the
539   segmentation overlay is from a deeper region of the tomogram than the EM image which is why the
540   lines of the segmentation and the overlay do not always align. **(B)** 3D segmented model. The
541   reconstruction is approximately 400 nm thick. Scale bar = 1000 nm. **(C)** 3D model showing the
542   distribution of cSR (yellow), the peripheral SR (purple) containing PCs near the sarcolemma (green
543   line, only segmented in a single plane). Sub-sarcolemmal mitochondria are also shown (cyan). The
544   free SR throughout the cell that connects PCs to the cSR has also not been segmented. Scale bar =
545   500 nm; scale in z-plane is approximately 400 nm.

546   **Fig. 2.** Peripheral couplings (PCs) and inter PC distances in the avian right ventricle. **(A, B)** Examples
547   of PCs (arrows) from tomograms identified as darkly stained SR cisternae that are closely opposed to

548   the sarcolemma. Scale bars = 50 nm in both panels. **(C)** The nearest edge-edge distances between

549   PCs in all four cardiac chambers. Scatter plots represent combined measurements for two birds (LV,

550   RV) or three birds (LA, RA) with mean ± s.e.m. overlaid. The * signifies that the RV was statistically

551   different to LA, RA, and LV via one-way ANOVA, with P<0.05. The number of distance measurements

552   between individual PCs are as follows: n = LA (380), RA (228), LV (193), RV (195).

553   **Fig. 3.** Corbular sarcoplasmic reticulum (cSR) in avian cardiomyocytes. **(A, B)** Examples of cSR

554   (arrows) from tomograms from right ventricle (A, scale bar = 100 nm) and left atrium (B, scale bar =

555   200 nm), identified as darkly stained SR cisternae found near Z-lines, roughly 100 nm in width. **(C)**

556   The nearest edge-edge distances between cSR along the same Z-line in all four cardiac chambers.

557   Scatter plots represent combined measurements for two birds (LV, RV) or three birds (LA, RA), with

558   mean ± s.e.m. overlaid. The * signifies that the LA was statistically different to RA (one-way ANOVA

559   P<0.05). The number of distance measurements between cSR are as follows: n= LA (286), RA (189),

560   LV (133), RV (194).

561   **Fig. 4.** Geometric models of the corbular sarcoplasmic reticulum (cSR) in avian myocardium. **(A)** 3D

562   segmented cSR (various colours). Scale bar = 1000 nm. **(B)** Isosurface rendering of an individual cSR

563   (arrow), attached to the free SR network. Scale bar = 100 nm. Scatterplots show the spread of the

564   data for **(C)** diameter, **(D)** surface area and **(E)** volume of individual cSR, in the 4 chambers of the

565   heart with mean ± s.e.m. overlaid. The same data is tabulated in Table S2. Measurements were

566   performed in all 4 chambers from a bird heart; n= LA (50), RA (40), LV (28), RV (26). Statistical

567   analyses showed LA statistically different to RV in (D) and LA statistically different to LV in (E).

568   **Fig. 5.** Simulated cell activation time and direction of Ca^{2+} wave propagation. **(A)** 2D model geometry

569   showing distance between CRUs. **(B)** Representative frames from a simulation of Ca^{2+} waves. Top

570   panel shows stimulation at cell membrane. In the middle and bottom panels, Ca^{2+} diffuses from Ca^{2+}

571   release sites to neighbouring sites and induces Ca^{2+} release at the neighbouring sites leading to

572   whole cell Ca^{2+} activation.

573

574   **Fig. 6.** Output of 2D avian cell model showing activation times (ms) as a function of d1, distance

575   between PCs **(A)**; and d3, distance between cSR along a Z-line **(B)**. Within each panel (i-iv) the

576   relationship is plotted as d2 (distance between Z-lines) is increased. The distance of d2 was varied to

577   represent Z-line spacing indicative of a myocyte at rest (1.7- 1.9 μm), as well as encompassing values

578   that could be achieved during myocardial stretch (2.1 μm) and during myocardial contraction (1.5

579 μm). In each graph, the circles represent the averaged result of 10 simulations. Each simulation

580 required 24 processors for 4 hours.

581

Figure 1
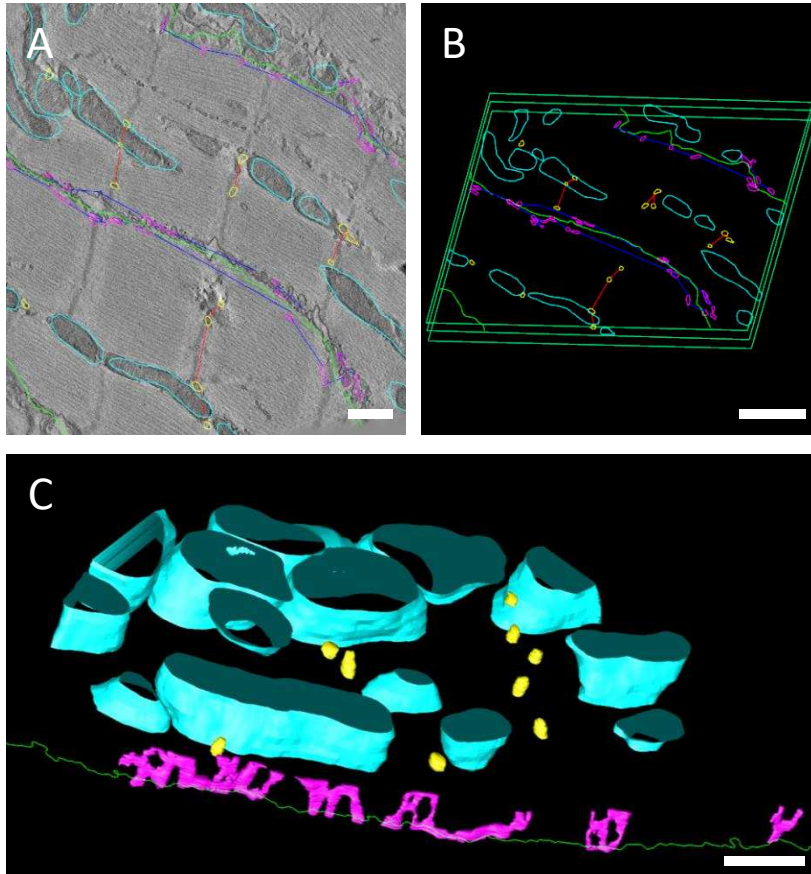
Fig. 1. Tomograms and segmented structural models used for measuring inter-CRU distances in avian left atrial tissue. **(A)** 2D image from a reconstructed tomogram stack, with a segmented model overlaid. The segmented model shows: peripheral couplings (PCs) (purple) and the nearest edge-edge distances between PCs (blue lines); corbular sarcoplasmic reticulum (cSR) (yellow) and the nearest edge-edge distances between these CRUs along a Z-line (red lines). Also segmented are the mitochondria (cyan) and the sarcolemma (green lines). Scale bar = 500 nm. **(B)** 3D segmented model. The reconstruction is approximately 400 nm thick. Scale bar = 1000 nm. **(C)** 3D model showing the distribution of cSR (yellow), the peripheral SR (purple) containing PCs near the sarcolemma (green line, only segmented in a single plane). Sub-sarcolemmal mitochondria are also shown (cyan). The free SR throughout the cell that connects PCs to the cSR has also not been segmented. Scale bar = 500 nm; scale in z-plane is approximately 400 nm.

Figure 2
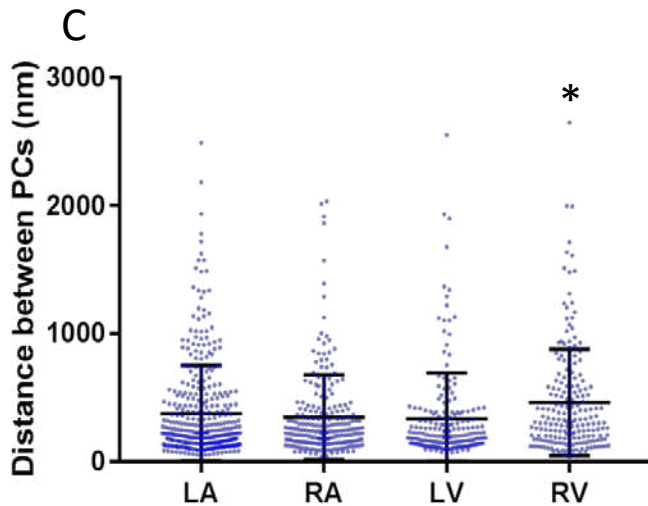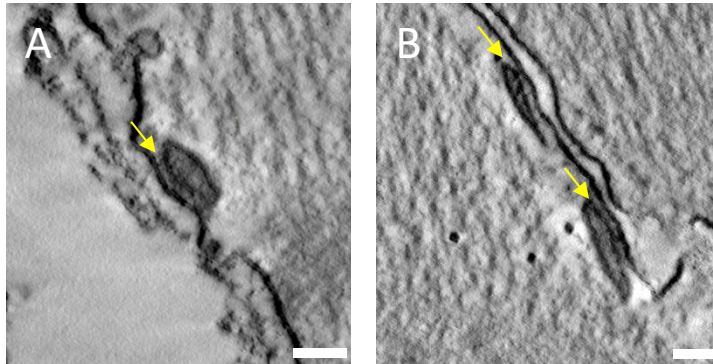
Fig. 2. Peripheral couplings (PCs) and inter PC distances in the avian right ventricle. **(A, B)** Examples of PCs (arrows) from tomograms identified as darkly stained SR cisternae that are closely opposed to the sarcolemma. Scale bars = 50 nm in both panels. **(C)** The nearest edge-edge distances between PCs in all four cardiac chambers. Scatter plots represent combined measurements for two birds (LV, RV) or three birds (LA, RA) with mean ± s.e.m. overlaid. The * signifies that the RV was statistically different to LA, RA, and LV via one-way ANOVA, with P<0.05. The number of distance measurements between individual PCs are as follows: n = LA (380), RA (228), LV (193), RV (195).

Figure 3
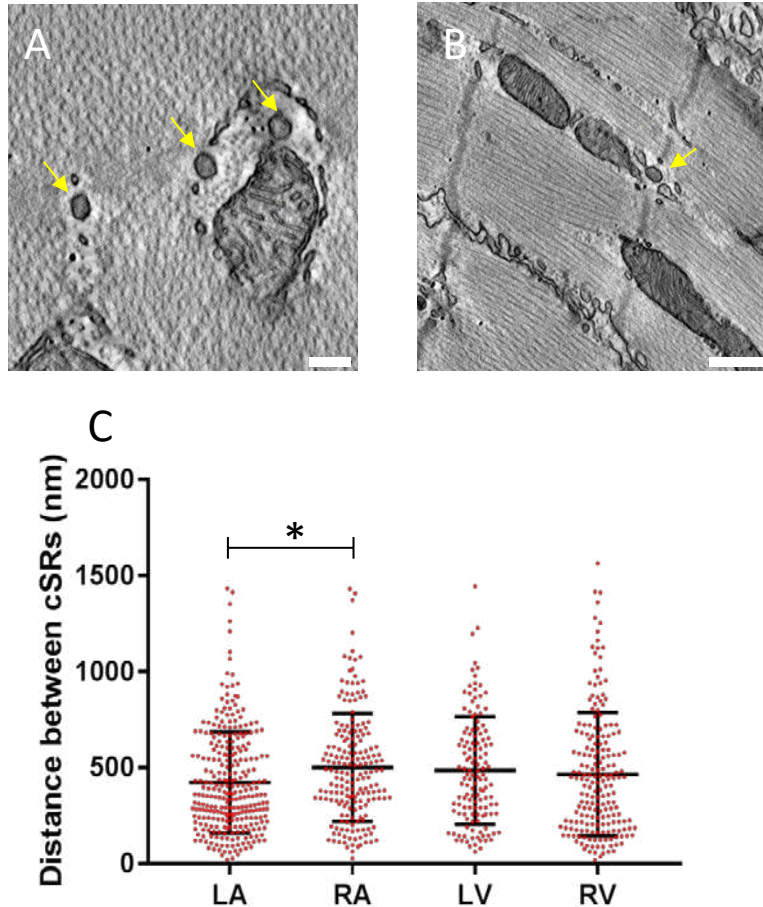
Fig. 3. Corbular sarcoplasmic reticulum (cSR) in avian cardiomyocytes. **(A, B)** Examples of cSR (arrows) from tomograms from right ventricle (A, scale bar = 100 nm**)** and left atrium (B, scale bar = 200 nm**)**, identified as darkly stained SR cisternae found near Z-lines, roughly 100 nm in width. **(C)** The nearest edge-edge distances between cSR along the same Z-line in all four cardiac chambers. Scatter plots represent combined measurements for two birds (LV, RV) or three birds (LA, RA), with mean ± s.e.m. overlaid. The * signifies that the LA was statistically different to RA (one-way ANOVA P<0.05). The number of distance measurements between cSR are as follows: n= LA (286), RA (189), LV (133), RV (194).

Figure 4
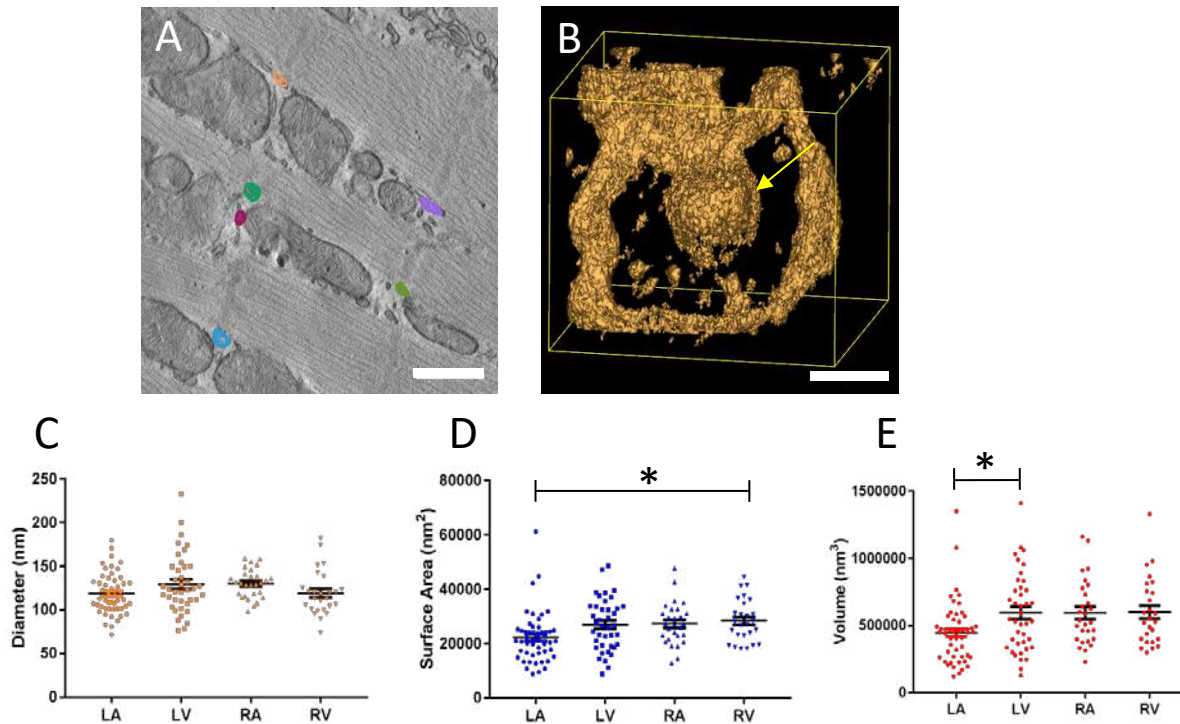
Fig. 4. Geometric models of the corbular sarcoplasmic reticulum (cSR) in avian myocardium. **(A)** 3D segmented cSR (various colours). Scale bar = 1000 nm. **(B)** Isosurface rendering of an individual cSR (arrow), attached to the free SR network. Scale bars = 100 nm. Scatterplots show the spread of the data for **(C)** diameter, **(D)** surface area and **(E)** volume of individual cSR, in the 4 chambers of the heart with mean ± s.e.m. overlaid. The same data is tabulated in Table S2. Measurements were performed in all 4 chambers from a bird heart; n= LA (50), RA (40), LV (28), RV (26). Statistical analyses showed LA statistically different to RV in (D) and LA statistically different to LV in (E).

Figure 5
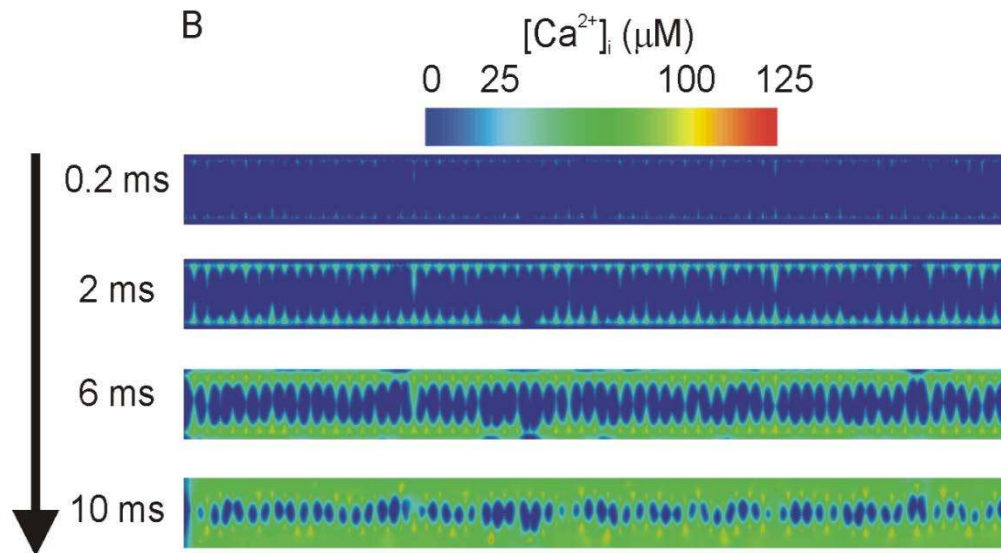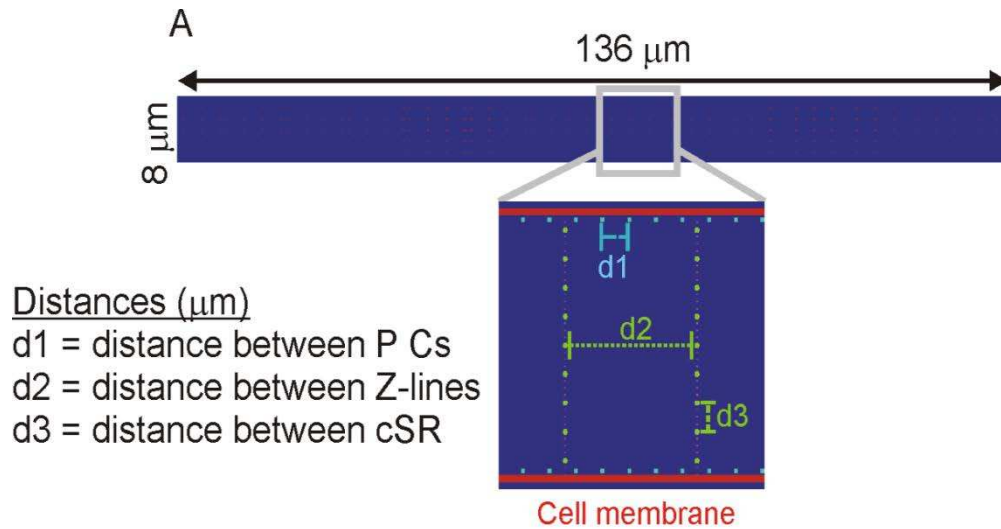
A

136 µm

8 µm

Distances (µm)
d1 = distance between P Cs
d2 = distance between Z-lines
d3 = distance between cSR

d1
d2
d3

Cell membrane

B

$[Ca^{2+}]_i$ (µM)

0   25   100   125

0.2 ms

2 ms

6 ms

10 ms

Fig. 5. Simulated cell activation time and direction of Ca^{2+} wave propagation. **(A)** 2D model geometry showing distance between CRUs. **(B)** Representative frames from a simulation of Ca^{2+} waves. Top panel shows stimulation at cell membrane. In the middle and bottom panels, Ca^{2+} diffuses from Ca^{2+} release sites to neighbouring sites and induces Ca^{2+} release at the neighbouring sites leading to whole cell Ca^{2+} activation.
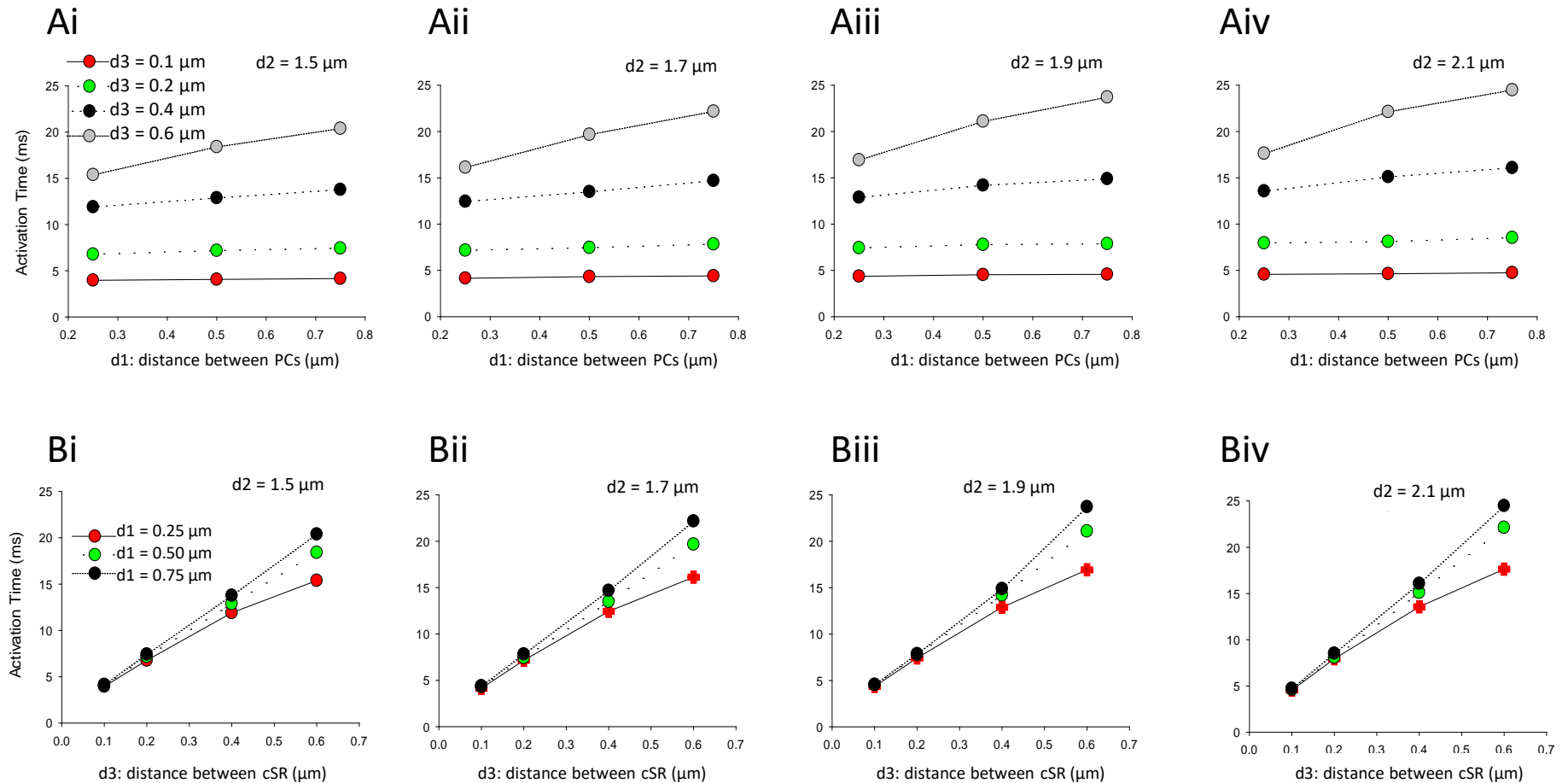
Fig. 6. Output of 2D avian cell model showing activation times (ms) as a function of d1, distance between PCs **(A)**; and d3, distance between cSR along a Z-line **(B)**. Within each panel (i-iv) the relationship is plotted as d2 (distance between Z-lines) is increased. The distance of d2 was varied to represent Z-line spacing indicative of a myocyte at rest (1.7- 1.9 μm), as well as encompassing values that could be achieved during myocardial stretch (2.1 μm) and during myocardial contraction (1.5 μm). In each graph, the circles represent the averaged result of 10 simulations. Each simulation required 24 processors for 4 hours.